View metadata, citation and similar papers at core.ac.uk
brought to you by CORE
provided by RERO DOC Digital Library

(CS#2014) doi: 10.7566/JPSCP.5.010001, 2015
which should be cited to refer to this work.

Competition between Energy-Dependent U and Nonlocal Self-Energy in Correlated Materials: Application of GW+DMFT to $SrVO_3$

R. Sakuma[1], Ph. Werner[2], and F. Aryasetiawan[1]

[1]*Department of Physics, Division of Mathematical Physics, Lund University, Sölvegatan 14A, 223 62 Lund, Sweden*
[2]*Department of Physics, University of Fribourg, 1700 Fribourg, Switzerland*

E-mail: ferdi.aryasetiawan@teorfys.lu.se

We describe an implementation of the GW+DMFT method and apply it to calculate the electronic structure of $SrVO_3$. Our results show that there is a strong competition between the frequency-dependent Hubbard U *and* the non-local self-energy via the GW approximation. It is crucial to take into account these two aspects in order to obtain an accurate and coherent picture of the quasi-particle band structure and satellite features of $SrVO_3$. Our main conclusion is that the GW+DMFT results for $SrVO_3$ are not attainable within the GW approximation or the LDA+DMFT scheme.

KEYWORDS: GW method, dynamical mean-field theory, GW+DMFT, strongly correlated electrons

http://doc.rero.ch

1. Introduction

The last few decades have witnessed a large amount of newly discovered and synthesized materials with many intriguing properties. A particular class of these materials are known as strongly correlated, meaning that conventional theories based on the one-electron or mean-field picture are found to be far from sufficient in describing their electronic structure. Perhaps the most well known example of this class of materials is the high-temperature superconducting copper oxides. The electronic structure of these materials is characterized by a set of partially filled narrow bands usually originating from 3d or 4f orbitals embedded in relatively broad bands which are well described within the one-particle picture. The narrow bands on the other hand pose a great theoretical difficulty because the Coulomb repulsion among electrons residing in those bands becomes comparable to or larger than the kinetic energy as measured by the band width. This leads to a failure of the mean-field picture and necessitates a proper treatment of the Coulomb repulsion. The usual approach to describe the electronic structure of these systems is to resort to model Hamiltonians, among the most famous are the Hubbard model and the Anderson impurity model. These models, however, require input parameters in the form of tight-binding hopping parameters and the Hubbard U. Describing the electronic structure of correlated materials fully from first principles is one of the great challenges in modern condensed matter physics.

The dynamical mean-field theory (DMFT) [1–3] in combination with the local density approximation (LDA), known as the LDA+DMFT scheme [4–7], provides in many cases a realistic description of the electronic structure and spectral functions of correlated materials. This method, however, suffers from a number of conceptual problems. One of them is the double-counting problem that arises from the difficulty in subtracting the contribution of the LDA exchange-correlation potential in the

correlated subspace. Another shortcoming is the DMFT assumption that the self-energy is local. A recent study based on the GW approximation (GWA) [8–11] indicates that even in correlated materials, such as $SrVO_3$, the non-local self-energy has a non-negligible influence on the electronic structure. In particular, it was found that the non-local self-energy widens the bandwidth significantly [12].

In this article we describe a procedure for carrying out calculations of the electronic structure of correlated materials from first principles. The procedure starts from selecting a subspace of the complete one-particle Hilbert space believed to be most relevant for the low-energy electronic structure. A downfolding method is then applied to determine the energy-dependent effective interaction among electrons residing in the chosen subspace. The chosen one-particle subspace together with the effective interaction provides a low-energy model which is solved using the DMFT method. The self-energy of the rest of the subspace is approximated within the GWA which is then combined with the impurity or DMFT self-energy leading to the GW+DMFT self-energy [13], after removing the double-counting term. The GW+DMFT self-energy is then free from double counting and preserves the non-locality or k-dependence of the GW self-energy.

The GW+DMFT scheme is illustrated by applying it to the much studied cubic perovskite $SrVO_3$, generally considered to be a prototype of correlated metals, as is evident from the large number of both experimental [14–22] and theoretical works [23–31], There are two main discrepancies of the LDA electronic structure when compared with experiment. Experimentally, a substantial t_{2g} band narrowing by a factor of two compared with the LDA bandwidth is observed [20]. In addition, there are satellite features a few eV below and above the Fermi level, interpreted as the lower and upper Hubbard bands [14–16, 20]. Intriguing kinks at low energies are also observed in photoemission experiments [22]. We will show that the GW+DMFT scheme is able to provide a consistent description of the electronic structure of $SrVO_3$ in agreement with the experimentally observed features.

2. Theory

2.1 Constrained RPA

We may divide the total polarisation of the system into the polarisation within the model subspace, which we shall call P_d, and the rest of the polarisation, which we shall call P_r. Accordingly

$$P = P_d + P_r. \tag{1}$$

The meaning of P_d and P_r is illustrated in Fig. 1. In the example of $SrVO_3$ in Fig. 2 the red curve correspond to the subspace of our model (d subspace) and we wish to determine the Hubbard U or the effective interaction among electrons residing in this subspace corresponding to vanadium t_{2g} band.

The fully screened Coulomb interaction is obtained by solving the following equation

$$W = v + vPW. \tag{2}$$

This equation can be rewritten as follows

$$W = W_r + W_r P_d W, \tag{3}$$

where W_r fulfils

$$W_r = v + vP_r W_r. \tag{4}$$

It can be readily verified by substituting (4) into (3) that (2) is recovered. We observe that the identity in Eq. (3) allows us to interpret W_r as the effective interaction among electrons residing in the model subspace or the Hubbard U [32] because when this effective interaction is screened further in the model by P_d we obtain the fully screened interaction:

http://doc.rero.ch

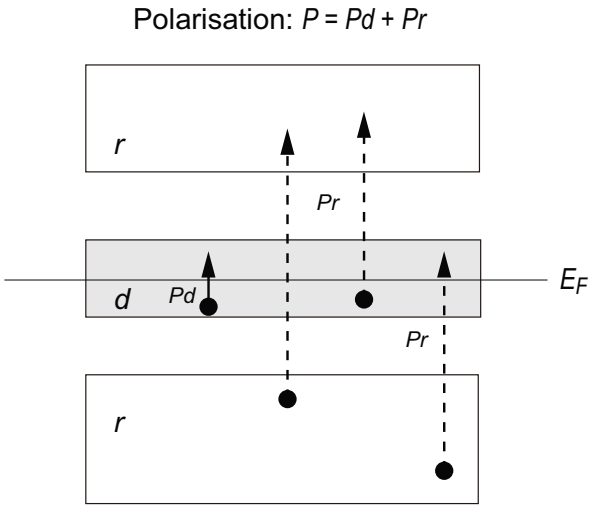

Fig. 1. A schematic picture depicting the meaning of P_d and P_r. While P_d is confined to the transitions within the d subspace, P_r may contain transitions between the d and r subspaces.

http://doc.rero.ch

$$U(\mathbf{r},\mathbf{r}';\omega) = W_r(\mathbf{r},\mathbf{r}';\omega). \tag{5}$$

As a consequence of retarded screening effects the Hubbard U is frequency dependent. A formal derivation of the Hubbard U from the many-electron Hamiltonian may be found in [33].

Eq. (4) is exact but in practice we approximate $P_r = P - P_d$ within the RPA, which takes the form

$$P(\mathbf{r},\mathbf{r}';\omega) = \sum_{kn}^{\text{occ}} \sum_{k'n'}^{\text{unocc}} \left\{ \frac{\psi^*_{kn}(\mathbf{r})\psi_{k'n'}(\mathbf{r})\psi^*_{k'n'}(\mathbf{r}')\psi_{kn}(\mathbf{r}')}{\omega - \varepsilon_{k'n'} + \varepsilon_{kn} + i\delta} - \frac{\psi_{kn}(\mathbf{r})\psi^*_{k'n'}(\mathbf{r})\psi_{k'n'}(\mathbf{r}')\psi^*_{kn}(\mathbf{r}')}{\omega + \varepsilon_{k'n'} - \varepsilon_{kn} - i\delta} \right\}, \tag{6}$$

where $\{\psi_{kn}, \varepsilon_{kn}\}$ are usually chosen to be the Kohn-Sham eigenfunctions and eigenvalues and $k = (\mathbf{k}, \sigma)$ is a combined index for the $\mathbf{k}$-vector and the spin σ. For systems without spin-flipping processes, k and k' evidently have the same spin. P_d has exactly the same form as in Eq. (6) but with the bands n and n' restricted to the d subspace. We note that P_r contains not only transitions inside the r subspace but also transitions between the d and r subspaces as illustrated in Fig. 1.

2.2 The GW+DMFT method

Although the GW+DMFT method was proposed more than a decade ago in Ref. [13] only very recently its implementation became possible. The reason for this is due to the appearance of energy-dependent Hubbard U in the impurity problem and only a few years ago an algorithm based on the continuous-time quantum Monte Carlo (CT-QMC) technique was invented to solve an impurity problem with dynamic U [34–39] which has made a proper implementation of the GW+DMFT scheme possible. Our calculations are based on the strong-coupling CT-QMC technique explained in Refs. [37] and [38].

The formalism of the GW+DMFT scheme is described in detail in an earlier publication [13]. Here we describe a practical implementation of the scheme. In the GW+DMFT scheme the total self-energy is given by the sum of the GW self-energy and the DMFT impurity self-energy with a

http://doc.rero.ch

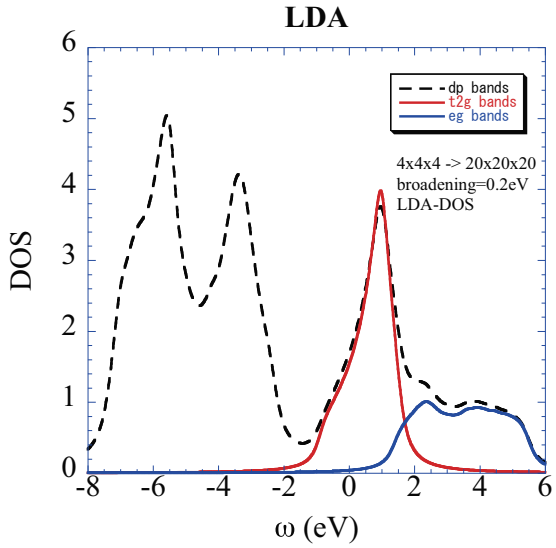

Fig. 2. The LDA density of states of $SrVO_3$. The red curve corresponds to the vanadium t_{2g} band.

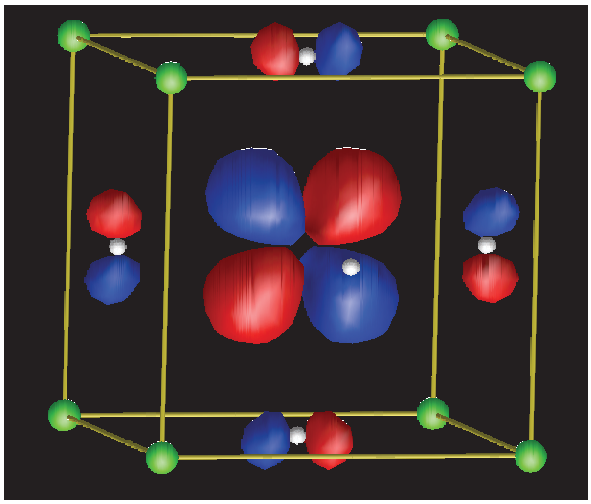

Fig. 3. The Wannier orbital corresponding to the vanadium 3d orbitals of t_{2g} character.

double-counting correction:

$$\hat{\Sigma}(\omega) = \sum_{\mathbf{k}nn'} |\psi_{\mathbf{k}n}\rangle \, \Sigma^{GW}_{nn'}(\mathbf{k},\omega) \, \langle\psi_{\mathbf{k}n'}| + \sum_{mm'} |\varphi_m\rangle \left[\Sigma^{\mathrm{imp}}_{mm'}(\omega) - \Sigma^{\mathrm{DC}}_{mm'}(\omega)\right] \langle\varphi_{m'}| \,, \tag{7}$$

where the $\{\psi_{\mathbf{k}n}\}$ are the LDA Bloch states and the $\{\varphi_m\}$ are the Wannier orbitals constructed from the vanadium t_{2g} bands. illustrated in Fig.3. The Wannier function centered at $\mathbf{R}$ is calculated as

$$\varphi_{m\mathbf{R}} = \frac{1}{N_{\mathbf{k}}} \sum_{\mathbf{k}\mu} e^{-i\mathbf{k}\cdot\mathbf{R}} S_{\mu m}(\mathbf{k}) \psi_{\mu\mathbf{k}}(\mathbf{r}) \tag{8}$$

where $S(\mathbf{k})$ is the transformation matrix that yields the maximally localized Wannier orbitals according to the prescription of Marzari and Vanderbilt [40,41]. We employ a recently proposed symmetry-constrained routine [42] to construct symmetry-adapted Wannier functions using a customized version of the Wannier90 library [43].The GW self-energy and the impurity self-energy are calculated separately, the latter is obtained from the LDA+DMFT scheme with dynamic U [35–37, 44]. The double-counting correction Σ^{DC} is the contribution of Σ^{GW} to the onsite self-energy which is already contained in the impurity self-energy Σ^{imp} calculated within the DMFT with dynamic U. The explicit formula for the double-counting correction is

$$\Sigma^{\mathrm{DC}}_{mm'}(\omega) = i \sum_{m_1 m_2 \subset t_{2g}} \int \frac{d\omega'}{2\pi} G^{\mathrm{loc}}_{m_1 m_2}(\omega+\omega') \times W^{\mathrm{loc}}_{mm_1,m_2m'}(\omega'), \tag{9}$$

where

$$G^{\mathrm{loc}}(\omega) = \sum_{\mathbf{k}} S^{\dagger}(\mathbf{k}) G(\mathbf{k},\omega) S(\mathbf{k}) \tag{10}$$

is the onsite projection of the lattice Green function of the t_{2g} subspace. In Eq. (9), W^{loc} is *not* the local part of the usual screened Coulomb interaction, but it is the screened interaction corresponding to the impurity problem in DMFT with the frequency-dependent interaction. The matrix elements of W^{loc} are

$$\begin{aligned} W^{\mathrm{loc}}_{mm_1,m_2m'}(\omega) = \int d^3r d^3r' \varphi^*_m(\mathbf{r}) \varphi_{m_1}(\mathbf{r}) W^{\mathrm{loc}}(\mathbf{r},\mathbf{r}';\omega) \\ \times \varphi^*_{m_2}(\mathbf{r}') \varphi_{m'}(\mathbf{r}'), \end{aligned} \tag{11}$$

and W^{loc} is obtained from

$$W^{\mathrm{loc}}(\omega) = \left[1 - U^{\mathrm{loc}}(\omega) P^{\mathrm{loc}}(\omega)\right]^{-1} U^{\mathrm{loc}}(\omega). \tag{12}$$

Here, $U^{\mathrm{loc}}(\omega)$ is the onsite Hubbard U of the impurity problem calculated using the constrained random-phase approximation (cRPA) [32] and $P^{\mathrm{loc}} = -iG^{\mathrm{loc}}G^{\mathrm{loc}}$ is the local polarization for each spin channel:

$$P^{\mathrm{loc}}(\mathbf{r},\mathbf{r}';\omega) = -i \int \frac{d\omega'}{2\pi} G^{\mathrm{loc}}(\mathbf{r},\mathbf{r}';\omega+\omega') G^{\mathrm{loc}}(\mathbf{r}',\mathbf{r};\omega'), \tag{13}$$

and G^{loc} is given in Eq. (10).

The quasi-particle band structure is obtained from the solution of

$$E_{\mathbf{k}n} - \varepsilon_{\mathbf{k}n} - \mathrm{Re}\Sigma_{nn}(\mathbf{k}, E_{\mathbf{k}n}) = 0, \tag{14}$$

where $\Sigma_{nn}(\mathbf{k},\omega) = \langle \psi_{\mathbf{k}n} | \hat{\Sigma}(\omega) | \psi_{\mathbf{k}n} \rangle$ and $\Sigma(\hat{\omega})$ is given in Eq. (7). In calculating the quasiparticle energies, the shift of the Fermi level is taken into account according to Hedin's prescription [45]. In a perturbative non self-consistent approach like G_0W_0, the mismatch of the Fermi energy between the initial and final states leads to unphysical broadening of quasiparticle peaks near the new Fermi energy. The prescription to solve this problem proposed by Hedin is to calculate the spectral function as [45]

$$A(\omega) = \frac{1}{\pi} \sum_{\mathbf{k}} \sum_{n} \frac{|\mathrm{Im}\Sigma_n(\mathbf{k},\omega-\Delta)|}{[\omega - \varepsilon_{\mathbf{k}n} - \mathrm{Re}\Sigma_n(\mathbf{k},\omega-\Delta)]^2 + [\mathrm{Im}\Sigma_n(\mathbf{k},\omega-\Delta)]^2}. \tag{15}$$

The energy shift Δ is given by

http://doc.rero.ch

$$\Delta = E_F - \varepsilon_F$$

where ε_F is the original LDA Fermi level and E_F is the new quasiparticle Fermi level. The shift Δ is determined self-consistently such that E_F obtained from

$$\int_{-\infty}^{E_F} d\omega A(\omega) = \text{electron number}$$

reproduces the starting Δ. The shift Δ makes sure that for $\omega = E_F$ we have

$$\text{Im}\,\Sigma_n(\mathbf{k}, E_F - \Delta) = \text{Im}\,\Sigma_n(\mathbf{k}, \varepsilon_F) = 0,$$

as it should be. Without the shift, $\text{Im}\,\Sigma$ calculated at the new Fermi level would not in general be zero and lead to a negative spectral function. In practice, we obtain Δ by calculating the self-energy shift for a state $\mathbf{k}n$ closest to ε_F:

$$\Delta = \text{Re}\Sigma_n(\mathbf{k}, E_{\mathbf{k}n} - \Delta) = \text{Re}\Sigma_n(\mathbf{k}, \varepsilon_{\mathbf{k}n}). \tag{16}$$

In this work, the LDA and *GW* calculations have been performed using the full-potential linearized augmented plane-wave codes FLEUR and SPEX [46, 47].

3. Application to $SrVO_3$

3.1 Quasi-particle band structure

We first consider the quasiparticle band dispersion. Angle-resolved photoemission (ARPES) measurements confirms the presence of well-defined quasi-particle band dispersion associated with t_{2g} symmetry and a broad almost structureless incoherent feature centered at -1.5 eV below the Fermi level [20]. From the slope of the band dispersion around the Fermi level, an estimated mass enhancement by a factor of 2 is found [20], consistent with the electronic specific-heat coefficient γ within the Fermi-liquid picture [15].

We compare in Fig. 4 the quasi-particle band structure obtained from several approaches. The bandwidth within LDA, *GW*, LDA+DMFT, and *GW*+DMFT are respectively 2.6, 2.1, 0.9, and 1.2 eV. It is well known that from the measured effective mass [15, 20], the LDA band width is a factor of two too large and one may then infer that the experimental bandwidth should be approximately 1.3 eV. The *GW* band width of 2.1 eV is significantly narrower than that of the LDA but still much too wide in comparison with the estimated experimental value. This result is in agreement with a recent work by Gatti and Guzzo [48] who also demonstrate that self-consistency within the so-called quasiparticle self-consistent *GW* (QSGW) scheme hardly alters the one-shot result and hence is not important in the case of $SrVO_3$. The bottom of the valence band within the GWA is found to be at 0.9 eV whereas experimentally it is about 0.6 eV.

Interestingly, the LDA+DMFT with dynamic U yields a quasi-particle bandwidth of 0.9 eV, which is too narrow compared with experiment. This result is well anticipated since the nonlocal self-energy, missing in the LDA+DMFT scheme, tends to widen the band, as pointed out in an earlier work [12]. With the inclusion of nonlocal self-energy within the *GW*+DMFT scheme, the bandwidth increases to 1.2 eV, in very close agreement with the experimental result. From ARPES data [20] the bottom of the occupied band is -0.6 eV, which is in good agreement with the *GW*+DMFT whereas the corresponding values for LDA, *GW*, and LDA+DMFT are respectively -1.0, -0.9, and -0.4 eV, as can be seen in Fig. 4. Unfortunately little experimental data is available for the unoccupied part of the band.

Intriguing kink features in the band dispersion were recently observed: a sharp kink at ~ 60 meV, likely of phonon origin, and a broad high-energy kink at ~ 0.3 eV below the Fermi level [22]. Since

http://doc.rero.ch

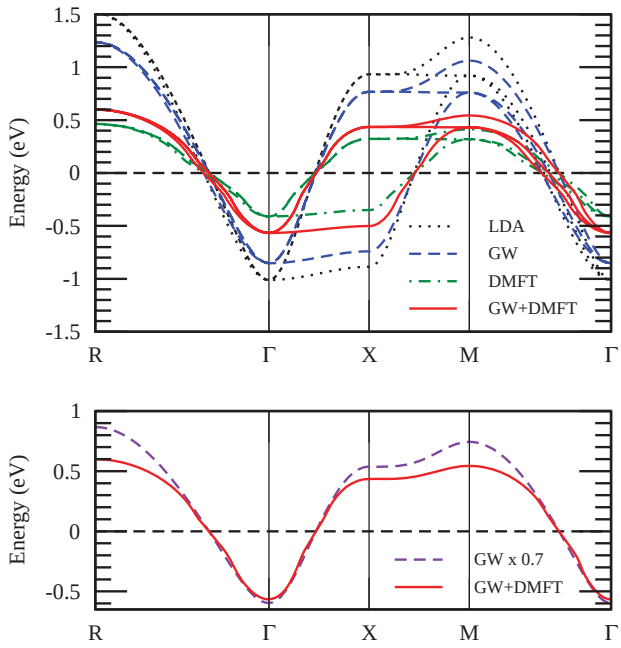

Fig. 4. (Color online) Upper panel: the quasi-particle band structure of $SrVO_3$ within LDA, *GW*, LDA+DMFT, and *GW*+DMFT. Lower panel: To emphasize the kink structure near Γ, the *GW*+DMFT band is plotted against a renormalized *GW* band. The figure is taken from Ref. [53].

http://doc.rero.ch

$SrVO_3$ is a Pauli-paramagnetic metal without any signature of magnetic fluctuations, the presence of a kink at high energy suggests a mechanism which is not related to spin fluctuations and it is explained as purely of electronic origin [27]. We also observe very weak but visible broad kinks between −0.1 and −0.4 eV in the vicinity of the Γ-point in the *GW*+DMFT band structure as can be seen in the lower panel of Fig. 4, where one of the *GW*+DMFT bands is plotted against a renormalized *GW* band, as was similarly done in Ref. [27]. The broad kinks can be recognized as deviations from a parabolic band. The origin of these kinks may be traced back to the deviation from a linear behavior of $\mathrm{Re}\,\Sigma$ between -0.5 and +0.5 eV.

3.2 Spectral functions

Angle-resolved photoemission (ARPES) measurements confirms the presence of a broad and almost structureless incoherent feature centered at −1.5 eV below the Fermi level [20], which may be interpreted as the lower Hubbard band. Inverse photoemission data reveals a satellite feature at around 2.5 eV above the Fermi level that may correspond to the upper Hubbard band.

The LDA density of states naturally does not show such satellite features since they originate from many-electron interactions. The *GW* spectral function on the other hand does contain satellite features but at too high binding energy, a well-known problem associated with the GWA. While the screened interaction contains the plasmon-like excitation at the right energy, the imaginary part of the *GW* self-energy places the peak at too high energy. The problem may be traced back to the GWA being first-order in the screened interaction *W*. The *GW*+DMFT spectra is shown in Fig. 5 where a broad lower Hubbard band is found centered at -1.5 eV, in agreement with a recent photoemission data by Yoshida *et al* [20]. No conclusive data are available for the upper Hubbard band but our theoretical calculation predicts its position at about 2 eV above the Fermi level. Calculations of the spectral functions within the *GW*+DMFT scheme for $SrVO_3$ have also been performed in Refs. [49,50].

3.3 Static vs *dynamic* U.

An issue which is only recently possible to address is the role of frequency dependence of the Hubbard U. It can be formally shown that downfolding the full many-body Hamiltonian to a low-energy model results in a frequency-dependent effective interaction [33]. The major effect of the dynamic U is the reduction in the quasi-particle weight or the Z-factor, as can be inferred from the slope of the self-energy along the Matsubara-axis at $\omega = 0$ [$Z \approx 1/(1 - \mathrm{Im}\Sigma(i\omega_0)/\omega_0)$], which is larger in the dynamic than the static U case. This reduction in the quasi-particle weight is due to the coupling to the high-energy plasmon excitations, missing in the static U calculation. This effect was first observed and discussed in the case of transition metal nickel within the GWA [32]. This increase in the slope of $\mathrm{Re}\,\Sigma$ or decrease in Z can be understood by writing the correlation part of $\mathrm{Re}\,\Sigma$ as a Hilbert transform:

$$\mathrm{Re}\,\Sigma(\omega) = \frac{1}{\pi}\int d\omega' \frac{|\,\mathrm{Im}\,\Sigma(\omega')|}{\omega - \omega'}.$$

The slope is given by

$$\frac{\partial\,\mathrm{Re}\,\Sigma}{\partial\omega} = -\frac{1}{\pi}\int d\omega' \frac{|\,\mathrm{Im}\,\Sigma(\omega')|}{(\omega - \omega')^2}.$$

Since the integrand is positive it is quite clear that additional weight in $\mathrm{Im}\,\Sigma$ due to the coupling to plasmon excitations will increase the magnitude of the slope around the Fermi level and decrease the Z-factor.

The reduction in the Z-factor due to the dynamic U results in a band narrowing. This band narrowing has been interpreted in a previous work [51] as the result of a two-step process: first the high-energy part of U renormalizes the one-particle LDA band via the self-energy and then the remaining low-energy U, which is approximately the static U, renormalizes these bands further, so that the final bandwidth is significantly narrower than the one obtained from just the static U. It was then argued that in order to obtain the same band narrowing as in the full calculation with dynamic U, the starting bandwidth should be reduced if the static cRPA U is to be used [51]. Indeed, to achieve the experimentally observed band narrowing a larger static U ($\sim$ 5 eV), compared with the static cRPA U of 3.4 eV, is needed in DMFT calculations. The larger static U however leads to an inconsistency: while the band narrowing or the mass enhancement is correct, the separation of the Hubbard bands becomes too large [26, 49]. For example, the lower Hubbard band came out too low at ~ -2.5 eV [26, 27].

The importance of dynamic U was also demonstrated recently in a study of the electronic structure of the superconductor iron-based pnictide $BaFe_2As_2$, in which the fequency dependence of U substantially modified the behavior of the self-energy around the Fermi level yielding an almost square-root like dependence of $\mathrm{Im}\,\Sigma(i\omega_n)$ along the Matsubara axis, in strong deviation from the linear dependence expected from the Fermi liquid theory [44].

4. Summary

In summary, we have performed calculations of the quasi-particle band structure as well as the spectral function of $SrVO_3$ within a simple version of GW+DMFT. While the bottom of the occupied GW band is too deep (-0.9 eV) and the DMFT with dynamic U too high (-0.4 eV), the GW+DMFT scheme yields a value of -0.6 eV, which is consistent with experimental data. From the point of view of the GWA the result illustrates the importance of onsite vertex corrections whereas from the DMFT point of view it demonstrates the significance of the non-local self-energy. A well-defined upper Hubbard band centered at around 2 eV is obtained whereas a rather broad incoherent feature is found below the quasi-particle peak centered at around -1.5 eV.

http://doc.rero.ch

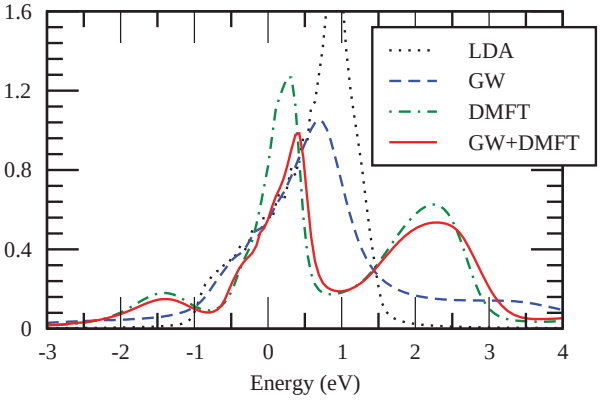

Fig. 5. (Color online) The total spectral function within LDA, GWA, LDA+DMFT, and *GW*+DMFT. The figure is taken from Ref. [53].

http://doc.rero.ch

The results also support the conclusion in a previous work [52] that there is a strong cancellation between the effects of momentum and energy dependence in the self-energy: The LDA+DMFT result with a dynamic U yields a band width narrower than the one obtained with a static U and inclusion of momentum dependence via the *GW* self-energy increases the band width. More detailed description of the work described in the present article may be found in Ref. [53].

Acknowledgments

We would like to thank C. Friedrich and S. Blügel for providing us with their FLAPW code and S. Biermann, M. Casula, and T. Miyake for fruitful discussions. This work was supported by the Swedish Research Council and "Materials Design through Computics: Complex Correlation and Non-Equilibrium Dynamics", a Grant in Aid for Scientific Research on Innovative Areas, MEXT, Japan, and by the Scandinavia-Japan Sasakawa Foundation. PW acknowledges support from SNF Grant No. 200021_140648. The computations were performed on resources from the Swedish National Infrastructure for Computing (SNIC) at LUNARC.

References

[1] W. Metzner and D. Vollhardt, Phys. Rev. Lett. **62**, 324 (1989).
[2] A. Georges and G. Kotliar, Phys. Rev. B **45**, 6479 (1992).
[3] A. Georges, G. Kotliar, W. Krauth, and M. J. Rozenberg, Rev. Mod. Phys. **68**, 13 (1996).
[4] V. I. Anisimov, A. I. Poteryaev, M. A. Korotin, A. O. Anokhin, and G. Kotliar, J. Phys. Cond. Matter **9**, 7359 (1997).
[5] A. I. Lichtenstein and M. I. Katsnelson, Phys. Rev. B **57**, 6884 (1998).
[6] G. Kotliar, S. Y. Savrasov, K. Haule, V. S. Oudovenko, O. Parcollet, C. A. Marianetti, Rev. Mod. Phys. **78**, 865 (2006).
[7] K. Held, Adv. Phys. **56**, 829 (2007).
[8] L. Hedin, Phys. Rev. **139**, A796 (1965).
[9] F. Aryasetiawan and O. Gunnarsson, Rep. Prog. Phys. **61**, 237 (1998).
[10] W. G. Aulbur, L. Jönsson, and J. W. Wilkins, Solid State Physics **54**, 1 (2000).
[11] G. Onida, L. Reining, and A. Rubio, Rev. Mod. Phys. **74**, 601 (2002).
[12] T. Miyake, C. Martins, R. Sakuma, and F. Aryasetiawan, Phys. Rev. B **87**, 115110 (2013).
[13] S. Biermann, F. Aryasetiawan, and A. Georges, Phys. Rev. Lett. **90**, 086402 (2003).
[14] K. Morikawa, T. Mizokawa, K. Kobayashi, A. Fujimori, H. Eisaki, S. Uchida, F. Iga, and Y. Nishihara, Phys. Rev. B **52**, 13711 (1995).
[15] I. H. Inoue, O. Goto, H. Makino, N. E. Hussey, and M. Ishikawa, Phys. Rev. B **58**, 4372 (1998).

http://doc.rero.ch

[16] A. Sekiyama, H. Fujiwara, S. Imada, S. Suga, H. Eisaki, S. I. Uchida, K. Takegahara, H. Harima, Y. Saitoh, I. A. Nekrasov, G. Keller, D. E. Kondakov, A. V. Kozhevnikov, Th. Pruschke, K. Held, D. Vollhardt, and V. I. Anisimov, Phys. Rev. Lett. **93**, 156402 (2004).

[17] T. Yoshida, K. Tanaka, H. Yagi, A. Ino, H. Eisaki, A. Fujimori, and Z.-X. Shen, Phys. Rev. Lett. **95**, 146404 (2005).

[18] R. Eguchi, T. Kiss, S. Tsuda *et al*, Phys. Rev. Lett. **96**, 076402 (2006).

[19] M. Takizawa, M. Minohara, H. Kumigashira, D. Toyota, M. Oshima, H. Wadati, T. Yoshida, A. Fujimori, M. Lippmaa, M. Kawasaki, H. Koinuma, G. Sordi, and M. Rozenberg, Phys. Rev. B **80**, 235104 (2009).

[20] T. Yoshida, M. Hashimoto, T. Takizawa, A. Fujimori, M. Kubota, K. Ono, and H. Eisaki, Phys. Rev. B **82**, 085119 (2010).

[21] K. Yoshimatsu, K. Horiba, H. Kumigashira, T. Yoshida, A. Fujimori, and M. Oshima, Science **333**, 319 (2011).

[22] S. Aizaki, T. Yoshida, K. Yoshimatsu, M. Takizawa, M. Minohara, S. Ideta, A. Fujimori, K. Gupta, P. Mahadevan, K. Horiba, H. Kumigashira, and M. Oshima, Phys. Rev. Lett. **109**, 056401 (2012).

[23] K. Maiti, D. D. Sarma, M. J. Rozenberg, I. H. Inoue, H. Makino, O. Goto, M. Pedio, and R. Cimino, Europhys. Lett. **55**, 246 (2001).

[24] A. Liebsch, Phys. Rev. Lett. **90**, 096401 (2003).

[25] E. Pavarini, S. Biermann, A. Poteryaev, A. I. Lichtenstein, A. Georges, and O. K. Andersen, Phys. Rev. Lett. **92**, 176403 (2004).

[26] K. Maiti, U. Manju, S. Ray, P. Mahadevan, I. H. Inoue, C. Carbone, and D. D. Sarma, Phys. Rev. B **73**, 052508 (2006).

[27] I. A. Nekrasov, K. Held, G. Keller, D. E. Kondakov, Th. Pruschke, M. Kollar, O. K. Andersen, V. I. Anisimov, and D. Vollhardt, Phys. Rev. B **73**, 155112 (2006).

[28] M. Karolak, T. O. Wehling, F. Lechermann, and A. I. Lichtenstein, J. Phys.: Condens. Matter **23**, 085601 (2011).

[29] M. Casula, A. Rubtsov, and S. Biermann, Phys. Rev. B **85**, 035115 (2012).

[30] H. Lee, K. Foyevtsova, J. Ferber, M. Aichhorn, H. O. Jeschke, and R. Valenti, Phys. Rev. B **85**, 165103 (2012).

[31] L. Huang and Y. Wang, Europhys. Lett. **99**, 67003 (2012).

[32] F. Aryasetiawan, M. Imada, A. Georges, G. Kotliar, S. Biermann, and A. I. Lichtenstein, Phys. Rev. B **70**, 195104 (2004).

[33] F. Aryasetiawan, J. M. Tomczak, T. Miyake, and R. Sakuma, Phys. Rev. Lett. **102**, 176402 (2009).

[34] A. N. Rubtsov, V. V. Savkin and A. I. Lichtenstein, Phys. Rev. B **72**, 035122 (2005).

[35] P. Werner, A. Comanac, L. de Medici, M. Troyer, A. J. Millis, Phys. Rev. Lett. **97**, 076405 (2006).

[36] P. Werner, A. J. Millis, Phys. Rev. B **74**, 155107 (2006).

[37] P. Werner, A. J. Millis, Phys. Rev. Lett. **99**, 146404 (2007).

[38] P. Werner, A. J. Millis, Phys. Rev. Lett. **104**, 146401 (2010).

[39] F. F. Assaad and T. C. Lang, Phys. Rev. B **76**, 035116 (2007).

[40] N. Marzari and D. Vanderbilt, Phys. Rev. B **56**, 12847 (1997).

[41] I. Souza, N. Marzari, and D. Vanderbilt, Phys. Rev. B **65**, 035109 (2001).

[42] R. Sakuma, Phys. Rev. B **87**, 235109 (2013).

[43] A. A. Mostofi, J. R. Yates, Y.-S. Lee, I. Souza, D. Vanderbilt, and N. Marzari, Comput. Phys. Commun. **178**, 685 (2008).

[44] P. Werner, M. Casula, T. Miyake, F. Aryasetiawan, A. J. Millis, and S. Biermann, Nature Physics **8**, 331 (2012).

[45] L. Hedin, J. Phys.: Condens. Matter **11**, R489 (1999).

[46] http://www.flapw.de/.

[47] C. Friedrich, S. Blügel, and A. Schindlmayr, Phys. Rev. B **81**, 125102 (2010).

[48] M. Gatti and M. Guzzo, Phys. Rev. B **87**, 155147 (2013).

[49] J. M. Tomczak, M. Casula, T. Miyake, F. Aryasetiawan, and S. Biermann, Europhys. Lett. **100**, 67001 (2012).

[50] C. Taranto, M. Kaltak, N. Parragh, G. Sangiovanni, G. Kresse, A. Toschi, and K. Held, Phys. Rev. B **88**, 165119 (2013).

[51] M. Casula, Ph. Werner, L. Vaugier, F. Aryasetiawan, T. Miyake, A. J. Millis, and S. Biermann, Phys. Rev. Lett. **109**, 126408 (2012).
[52] R. Sakuma, T. Miyake, and F. Aryasetiawan, Phys. Rev. B **86**, 245126 (2012).
[53] R.Sakuma, Ph. Werner, and F. Aryasetiawan, Phys. Rev. B **88**, 235110 (2013).

http://doc.rero.ch